ESKİŞEHİR TEKNİK ÜNİVERSİTESİ BİLİM VE TEKNOLOJİ DERGİSİ C- YAŞAM BİLİMLERİ VE BİYOTEKNOLOJİ

Eskişehir Technical University Journal of Science and Technology C- Life Sciences and Biotechnology

2023, 12(1), pp. 8-18, DOI:10.18036/estubtdc.1184733

RESEARCH ARTICLE

COMPARATIVE FLUX BALANCE ANALYSES OF SERINE ALKALINE PROTEASE OVERPRODUCTION IN *Bacillus subtilis* AT GENOME AND SMALL SCALE

Pınar KOCABAŞ *

* Bioengineering Department, Engineering Faculty, Ege University, İzmir, Turkey

ABSTRACT

This work aims to conduct flux balance analysis of serine alkaline protease overproduction in *Bacillus subtilis* using enzyme-constrained genome scale model and to compare the results with fluxes obtained from a smaller, bioreaction-based model. Fluxes of the enzyme constraint genome scale model were calculated using CobraToolbox v3.0 and compared with those of bioreaction-based model for the specific growth rate of zero. The active reaction number first increased and then remained constant with specific growth rate for enzyme constrained genome scale model. The SAP synthesis flux increased with a decrease in specific growth rate for both models. The TCA cycle was active for both models, but with lower fluxes for enzyme-constrained genome scale model. Anaplerotic reactions were active only for bioreaction-based model. Glycolysis pathway fluxes were active for enzyme-constrained genome scale model, meanwhile gluconeogenesis pathway fluxes were active for bioreaction-based model. Oxidative pentose phosphate pathway was inactive for both models and generally higher pentose phosphate pathway fluxes were obtained using bioreaction-based model. The fluxes toward amino acid synthesis pathways and serine alkaline protease synthesis were higher with bioreaction-based model. Since TCA cycle fluxes were lower with enzyme constrained genome scale model, ATP synthesis was lower with enzyme constrained genome scale model compared to bioreaction-based model. For both models, active pathways were the same for TCA cycle, pentose phosphate pathway, amino acid synthesis pathways except glycolysis pathway. The results showed that bioreaction-based model gave more sound results compared to enzyme constrained genome scale model since gluconeogenesis should be active with the carbon source of citrate.

Keywords: Enzyme constrained genome scale metabolic model, Metabolic flux analysis, Bioreaction-based model

Abbreviations

A: Stoichiometric matrix of the metabolic network
ATPS4r: adp[c]+4h[e]+pi[c]⇔ atp[c]+h2o[c]+3h[c]
ala_L[c]: Intracellular L-alanine
arg_L[c]: Intracellular L-arginine
asn_L[c]: Intracellular L-asparagine
asp_L[c]: Intracellular L-aspartate
atp[c]: Intracellular atp
adp[c]: Intracellular adp
BsBRM-2000: Bioreaction-based model [1]
c(t): Metabolite accumulation vector
$\mathbf{c_1(t)}$: Extracellular metabolite accumulation vector
$\mathbf{c_2(t)}$: Intracellular metabolite accumulation vector
$[E_j]$: $Concentration\ of\ enzyme\ j$
ec_iYO844: Enzyme constrained GEM [2]
ec_iYO844-SAP: SAP synthesis reaction [1] and exchange reaction for SAP were added to ec_iYO844 [2] forming ec_iYO844-SAP in this study
EX_SAP(e): SAP exchange reaction
FB: Flux balance
FBA: Flux balance analysis

*Corresponding Author: pinar.kocabas@ege.edu.tr
Received: 30.09.2022 Published: 30.01.2023

gln_L[c]: Intracellular L-glutamine
glu_L[c]: Intracellular L-glutamate
gly[c]: Intracellular glycine
GEM: Genome scale metabolic model
GECKO: Enzymatic Constraints using Kinetic and Omics data
his_L[c]: Intracellular L-histidine
ile_L[c]: Intracellular L-isoleucine
iYO844: *Bacillus subtilis* GEM [3]
leu_L[c]: Intracellular L-leucine
lys_L[c]: Intracellular L-lysine
met_L[c]: Intracellular L-methionine
PPP: Pentose phosphate pathway
PYK: adp[c]+h[c]+pep[c]=>atp[c]+pyr[c]
PGK: 13dpg[c]+adp[c]+8.44309e-07PM_PGK_f ⇔3pg[c]+atp[c]
phe_L[c]: Intracellular L-phenylalanine
pro_L[c]: Intracellular L-proline
pi[c]: Intracellular phosphate
r(t): reaction rate vector
k_{cat}^{j}: Turnover number of enzyme j
SAP: Serine alkaline protease
SAP: SAP synthesis reaction
SAP[e]: Extracellular SAP
ser_L[c]: Intracellular L-serine
thr_L[c]: Intracellular L-threonine
trp_L[c]: Intracellular L-tryptophan
tyr_L[c]: Intracellular L-tyrosine
v_j: $Rate\ of\ reaction\ j$
val_L[c] : Intracellular L-valine

1. INTRODUCTION

Genome scale metabolic models (GEMs) aim to describe the whole metabolism of an organism [4], containing: stochiometric reaction network and gene-protein-reaction-metabolite associations. Functions of GEMs are calculation of intracellular reaction rates in bioprocesses; determination of bottleneck reactions in bioreaction network; increasing yield and selectivity of bioprocesses by changing medium components, bioreactor operation parameters, microorganism or genetic structure; prediction of the results of genetic and environmental changes; determination of the maximum theoretical yield; generation of hypotheses, model-driven discovery; metabolic engineering and strain design [5-6].

Bacillus is an important group of industrial microorganisms acting as microbioreactors in fermentors [5]. *Bacillus subtilis* is the best defined Gram-positive bacteria [2]. *B.subtilis* genome was sequenced and updated totally over the last 20 years by many researchers [7-11], proven to be a model organism for systems biology. Progress in genome sequencing and consequently annotation studies results with reconstructing GEMs with more accurate gene-enzyme-reaction data and therefore with more accurate prediction capacity. There are six basic *B.subtilis* GEMs [12] apart from ec_iYO844 [2]. The first three GEMs are reconstructed with the biochemical and genomic knowledge based on genome sequencing of [7]. Therefore, they are called first generation *B.subtilis* GEMs [3, 13-14]. Second generation *B.subtilis* GEMs [15-16] are based on the genome sequencing of [8]. *i*Bsu1144 [12] is a third generation *B.subtilis* GEM that takes its genome annotation from [9] and ec_iYO844 [2] is a first generation *B.subtilis* GEM since it is based on [3].

Serine alkaline protease (SAP), one of the major industrial enzyme [5] is produced by *Bacillus sp*. at the start of stationary phase of growth [1]. Aims of this work are to conduct flux balance analysis of SAP overproduction in *Bacillus subtilis* using ec_iYO844-SAP that contains 1269 reactions, 1010 metabolites and to compare the results with those of biochemical reaction based model having 147 reactions and 105 metabolites [1] to assess validity of enzyme constrained GEM.

2. MATERIAL AND METHODS

2.1 Flux Balance Analyses

Stream of metabolites in a mathematically represented bioreaction network is computed with flux balance (FB) methodology to analyze metabolic flux distributions. The FB methodology cannot predict metabolite concentrations since it doesn't use kinetic parameters. Using fermentation data as constraints, an allowable solution space is obtained. FBA can determine a single optimum flux distribution on the edge of the allowable solution space by optimizing an objective function [12].

Mass-balance based stoichiometric equations are constructed for each metabolite in the cell, which is considered as a semi-batch microbioreactor. The algebraic sum of all conversion reactions of each metabolite-*i* in the defined reactions plus the transport of metabolite-*i* are equal to the accumulation of metabolite-*i* [6]. The scalar flux balance equations can be shown as a linear vector as follows:

$$A \times r(t) = c(t) \quad (1),$$

Where A is mxn stoichiometric coefficients matrix, m is the number of metabolites and n is the number of reactions [6], r(t) is the flux vector and c(t) is the metabolite accumulation vector. The elements of c(t) are two sub-vectors:

$$c(t)=c_1(t) + c_2(t) \quad (2)$$

where $c_1(t)$ and $c_2(t)$ correspond to extracellular and intracellular metabolite accumulation vectors, respectively. Using pseudo steady state (PSS) approximation for the intracellular metabolites, $c_2(t)$ is set to zero. Intracellular fluxes can be calculated by minimizing or maximizing the objective function Z, specified for a selected component-*i* [17].

$$Z=\sum \alpha_i . r_i \quad (3)$$

where, Z is a linear combination of fluxes (r_i) multiplied by the corresponding stoichiometric coefficient of component-*i* (α_i) for every reaction [12].

In this work, firstly SAP synthesis reaction [1] and exchange reaction for SAP were added to ec_iYO844 [2] forming ec_iYO844-SAP**.** Secondly, the objective function was defined as the exchange reaction of SAP in the cells; whereupon, maximization of the objective function was carried out at citrate's uptake rate at 10 mmole/g_{DW}/h and at various growth rates (μ=0, 0.05, 0.15, 0.25, 0.35, 0.45, 0.55, 0.65, 0.75 h^{-1}) using CobraToolbox v3.0 [18] to determine intracellular reaction rates. Reaction fluxes of metabolites are expressed in mmole/g_{DW}/h; and the flux towards the cell is the specific growth rate, μ(h^{-1}) [12].

2.2 Enzyme Constrained Genome Scale Metabolic Model

The enzymes that catalyze a reaction affect the metabolic flux. Different approaches have been developed to constrain the solution space and improve phenotypic predictions by integrating enzyme concentrations [2]. **GECKO** is the most promising method, using enzymatic data as a new constraint for each metabolic flux, provided that fluxes do not exceed the maximum capacity in a given condition [2, 19].

A set of available enzyme constraints (absolute protein levels and turnover numbers) for the reactions of central carbon metabolism were integrated into the iYO844 GEM of *B. subtilis* [3] following the

principles of the GECKO [2]: An additional constraint that the metabolic flux through the j-th reaction (R_j) does not exceed its maximum capacity (v_{max}), corresponding to the product between the k_{cat} value (converted to h^{-1}) of the enzyme E_j (that catalyzes the j-th reaction) and its abundance [E_j], as shown in Eq 4, was considered to implement the GECKO approach [2].

$$v_j \leq k_{cat}^{j} * [E_j] \qquad \text{for} \quad j=1\ldots17 \tag{4}$$

In this work ec_iYO844-SAP was constructed: Serine alkaline protease (SAP) synthesis reaction [1] (the reaction named as **SAP**) and exchange reaction for SAP (named as **EX_SAP(e)**) were added to ec_iYO844 [2] forming ec_iYO844-SAP containing 1269 reactions and 1010 metabolites. Since the system is underdetermined, optimization was carried out by maximizing the exchange reaction for SAP. SAP synthesis reaction was not chosen as the objective function since it yielded zero SAP production. Citrate uptake rate was considered as 10 mmole/g_{DW}/hr during flux balance analyses, which was conducted in CobraToolbox v3.0 [18]. The reason why citrate was chosen as the carbon source was that the aim of this study is to compare prediction capacities of a genome scale model and biochemical reaction-based model [1], which is named as BsBRM-2000 in this study for intracellular reaction rates/fluxes. Since there is already flux data obtained by theoretical capacity analysis conducted with BsBRM-2000 [1] taking citrate as the sole carbon source with its uptake rate as 10 mmole/g_{DW}/h [1], citrate was chosen to be carbon source.

Added reaction names and reactions are shown below:

SAP: 40 ala_L[c] + 4 arg_L[c] + 18 asn_L[c] + 9 asp_L[c] + 1096 atp[c] + 7 gln_L[c] + 5 glu_L[c] + 35 gly[c] + 5 his_L[c] + 10 ile_L[c] + 16 leu_L[c] + 9 lys_L[c] + 5 met_L[c] + 4 phe_L[c] + 10 pro_L[c] + 32 ser_L[c] + 20 thr_L[c] + 1 trp_L[c] + 13 tyr_L[c] + 31 val_L[c] -> 1096 pi[c] + 1096 adp[c] + SAP[e]

EX_SAP(e): SAP[e] ->

3. RESULTS

Theoretical capacity analysis led to optimized SAP overproduction by using a linear constrained optimization technique for several specific growth rates was conducted and the variation of the fluxes were calculated by fixing the sole carbon source citrate's uptake rate at 10 mmole/g_{DW}/h [1]. The objective function Z was defined as synthesis rate of SAP in the cells, whereupon optimum flux distributions were obtained by maximizing the objective function Z [1]. In this work, it was also aimed to conduct theoretical capacity analysis with ec_iYO844-SAP using the same citrate uptake rate, growth rates and however with different optimization functions (Exchange reaction for SAP, **EX_SAP(e)**) and compare the results with those of literature [1]. In this work, when the optimization function was taken as SAP synthesis reaction, there were no SAP synthesis in all growth rates. Therefore, exchange reaction for SAP was taken as optimization function since it yielded decreasing SAP synthesis with increasing specific growth rates as it was reported [1]. The mathematical model of [1], which is a bioreaction-based model, is named as BsBRM-2000 in this study (Table 1). Prediction capacities of a genome scale model and biochemical reaction-based model for intracellular reaction rates/fluxes were compared for the first time in this study.

Intracellular reaction rates were calculated for ec_iYO844-SAP for different growth rates. Fluxes of common reactions were compared for ec_iYO844-SAP and BsBRM-2000. Active reaction number first increased with growth rate and then remained constant with μ for ec_iYO844-SAP (Table 2). For both models, SAP synthesis rate decreased with growth rate; meanwhile, SAP synthesis flux was higher with BsBRM-2000 (Table 3). The flux ratio of SAP synthesis in two models increased with growth rate (Table 3).

Table 1. Comparison of models.

Gene #	**Reaction #**	**Metabolite #**	**Model**
844	1269	1010	ec_iYO844-SAP
-	147	105	BsBRM-2000

Table 2. Number of active reactions with ec_iYO844-SAP.

μ, h^{-1}	ec_iYO844-SAP	
	Active reaction #	% percent
0	162	12.8
0.05	351	27.7
0.15	351	27.7
0.25	351	27.7
0.35	351	27.7
0.45	351	27.7
0.55	351	27.7
0.65	-	-
0.75	-	-

Table 3. SAP synthesis fluxes.

μ, h^{-1}	Intracellular SAP flux (mmole/g_{DW}/h)		Flux ratio
	ec_iYO844-SAP	BsBRM-2000	
0.0	0.01511	0.0260	1.7
0.05	0.0139	0.0243	1.7
0.15	0.01148	0.0209	1.8
0.25	0.009056	0.0175	1.9
0.35	0.006635	0.0143	2.2
0.45	0.004215	0.0107	2.5
0.55	0.001795	0.0073	4.1
0.65	-	0.0039	-
0.75	-	0.0006	-

TCA cycle fluxes increased with growth rate for ec_iYO844-SAP (Figure 1), while TCA cycle fluxes did not change considerably with respect to growth rate for BsBRM-2000 [1]. Anaplerotic reactions were inactive for ec_iYO844-SAP (Figure 2). Glycolysis pathway fluxes increased with growth rate (Figure 3), oxidative PPP fluxes were inactive for ec_iYO844-SAP (Figure 4).

Fluxes toward serine-group, alanine- group, histidine, aromatic acid- group amino acid pathways decreased at least 1.2- fold with growth rate; meanwhile SAP synthesis flux decreased 8.4- fold with respect to growth rate (Table 4). There were similar decreases with BsBRM-2000 fluxes towards amino acid synthesis pathways (AAP) [1]. ATP synthesis rate increased 2.44- fold with growth rate for ec_iYO844-SAP (Table 5), meanwhile it did not change considerably for BsBRM-2000 [1]. Comparison of two models was carried out only for μ=0 h^{-1} since Çalık et al.[1] reported only central pathway fluxes for μ=0, 0.75 h^{-1} values and ec_iYO844-SAP was infeasible with μ=0.75 h^{-1}. The TCA cycle was active for both models similarly but with lower fluxes of ec_iYO844-SAP (Figure 5). Anaplerotic reactions were active only with BsBRM-2000 (Figure 6).

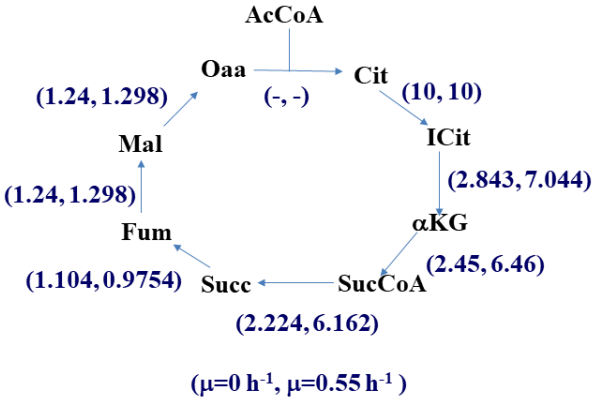

Figure 1. Effects of growth rate on TCA cycle fluxes (mmole/g_{DW}/hr) in SAP production calculated with ec_iYO844-SAP.

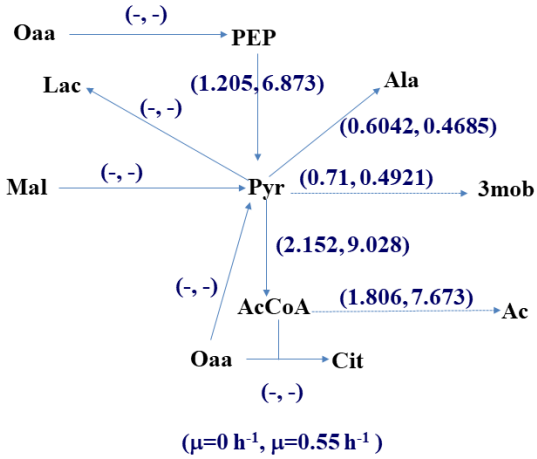

Figure 2. Effects of growth rate on Pyr node fluxes (mmole/g_{DW}/hr) in SAP production calculated with ec_iYO844-SAP.

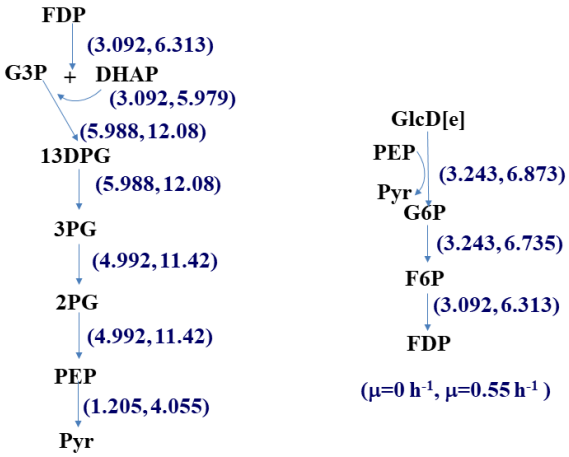

Figure 3. Effects of growth rate on glycolysis pathway fluxes (mmole/g_{DW}/hr) in SAP production calculated with ec_iYO844-SAP.

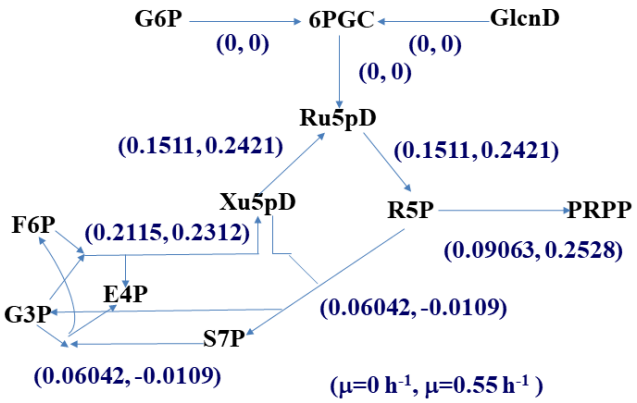

Figure 4. Effects of growth rate on PPP fluxes (mmole/g_{DW}/hr) in SAP production calculated with ec_iYO844-SAP.

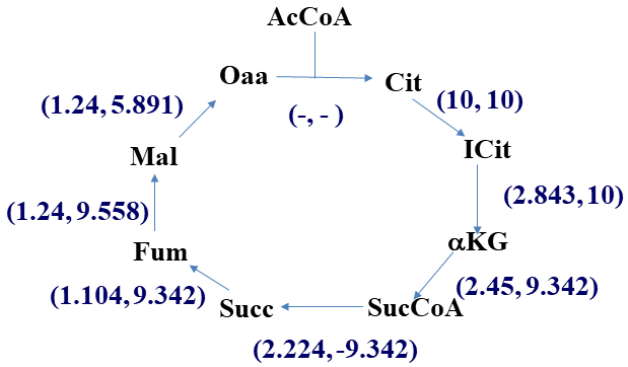

Figure 5. Comparison of TCA cycle fluxes (mmole/g_{DW}/h) in SAP production calculated with ec_iYO844-SAP and BsBRM-2000 for μ=0 h^{-1}, respectively.

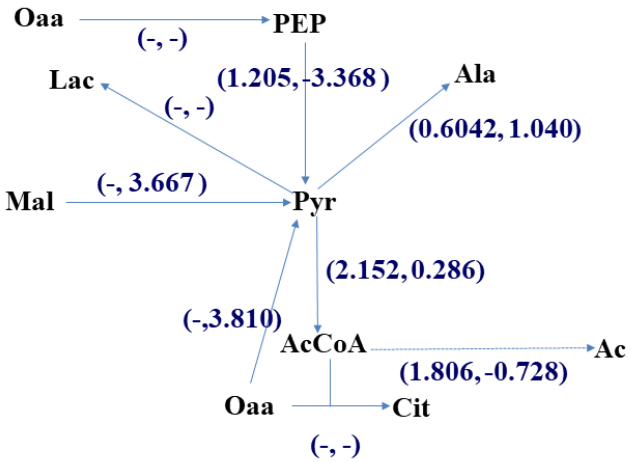

Figure 6. Comparison of Pyr node fluxes (mmole/g_{DW}/h) in SAP production calculated with ec_iYO844-SAP and BsBRM-2000 for μ=0 h^{-1}, respectively.

Table 4. Fluxes towards amino acid synthesis pathways, mmole/g_{DW}/h.

Amino acid synthesis pathways	μ=0 h^{-1}	μ=0.55 h^{-1}	Fold change
Serine group amino acid pathways	0.9959	0.6578	1.5↓
Alanine group amino acid pathways	0.6042	0.4685	1.3↓
Histidine synthesis	0.07553	0.05393	1.4↓
Aspartic acid group amino acid pathways	1.24	1.298	1
Aromatic group amino acid pathways	0.2719	0.2203	1.2↓

Table 5. Effects of growth rate on ATP synthesis fluxes in SAP production calculated with ec_iYO844-SAP.

Reaction	ATP synthesis, mmole/g_{DW}/h	
	μ=0 h^{-1}	μ=0.55 h^{-1}
PYK	1.205	4.055
ATPS4r	20.81	52.24
PGK	5.988	12.08
Total	28.003	68.375

Glycolysis pathway fluxes were active for ec_iYO844-SAP, meanwhile gluconeogenesis pathway fluxes were active for BsBRM-2000 at μ=0 h^{-1} [1]. Oxidative PPP was inactive for both models and generally higher PPP fluxes were obtained with BsBRM-2000 (Figure 7). The fluxes toward amino acid synthesis pathways and SAP synthesis were higher for BsBRM-2000 (Table 6). Since TCA cycle fluxes were lower with ec_iYO844-SAP, ATP synthesis was lower with ec_iYO844-SAP compared to BsBRM-2000 (Table 7).

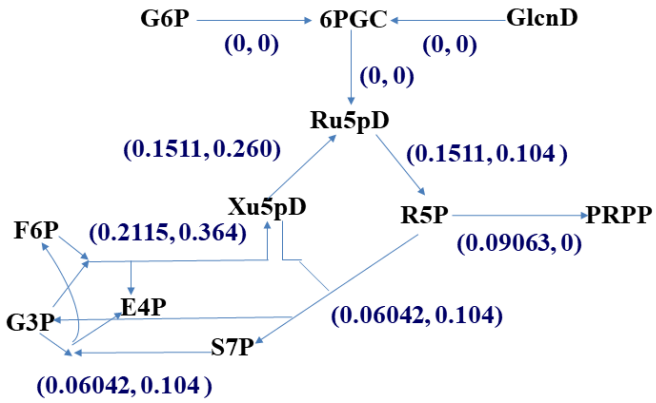

Figure 7. Comparison of PPP fluxes (mmole/g_{DW}/h) in SAP production calculated with ec_iYO844-SAP and BsBRM-2000 for μ=0 h^{-1}, respectively.

Table 6. Comparison of fluxes (mmole/g_{DW}/h) toward amino acid synthesis pathways in SAP production for μ=0 h^{-1}.

Amino acid synthesis pathways	ec_iYO844-SAP	BsBRM-2000	Fold change
Serine-group amino acid pathways	0.9959	1.573	1.6
Alanine-group amino acid pathways	0.6042	1.040	1.7
Histidine synthesis	0.07553	0.130	1.7
Aspartic acid- group amino acid pathways	1.24	2.081	1.7
Aromatic- group amino acid pathways	0.2719	0.273	1.0
Glutamic acid- group amino acid pathways	3.761	7.763	2.1

Table 7. Total ATP synthesis fluxes, mmole/g_{DW}/h: Comparison of ATP synthesis fluxes in SAP production for μ=0 h^{-1}.

ec_iYO844-SAP	BsBRM-2000	Fold change
28.003	52.46	1.9

4. DISCUSSION AND CONCLUSIONS

According to ec_iYO844-SAP and BsBRM-2000 results, active pathways were the same for TCA cycle, PPP and amino acid synthesis pathways except glycolysis pathway. Divergence of fluxes at glycolysis pathway was because enzyme-constraint GEM allows for glucose exchange, otherwise central carbon pathways were inactive with no SAP production at μ=0 h^{-1} with ec_iYO844-SAP. Citrate exerts a negative feedback on glycolysis by inhibiting phosphofructokinase 1 and 6-phosphofructo-2-kinase/fructose-2,6-biphosphatases (PFK2); on the contrary it stimulates pathways consuming ATP such as gluconeogenesis and lipid synthesis [20]. BsBRM-2000 yielded more sound results since an active gluconeogenesis pathway is expected with citrate as sole carbon source.

The number of active reactions increased with respect to growth rate and was maximum as 351. The minimum number of active reactions was 162 at μ=0 h^{-1} as anticipated since stationary phase implies less maintenance energy and less active metabolism inside the cell. This result was in harmony with the literature [21] where active reactions were calculated to be 322, 318, 43 for *Bacillus subtilis* (rBsP) in Period I (0<t<4h), Period II (4<t<12h), Periods III-V (12<t<32 h) calculated using GEM of iYO844 using glucose as carbon source, respectively. The number of active reactions at stationary phase calculated with enzyme constrained iYO844 (ec_iYO844-SAP) is 162, while the number of active reactions at stationary phase calculated with iYO844 [21] is 43 since different carbon sources were utilized in both models.

A bigger model does not necessarily yield better results as it was depicted in this study. The bioreaction - based model produced more sound results probably due to better connectivity. ec_iYO844-SAP could describe the changes in central carbon metabolism with growth rate in a better way. The number of enzyme-constrained reactions is 17 [2] although ec-iYO844-SAP has 1269 reactions and 1010 metabolites. If the number of enzyme-constrained reactions were 1269 for ec-iYO844-SAP, the actual metabolism could have been better depicted with ec-iYO844-SAP. Results will be convergent as more *Bacillus subtilis* reactions are discovered; enzyme information and intracellular regulations are integrated into GEMs.

CONFLICT OF INTEREST

The author confirms to have no competing financial interests or relationships that could influence the work reported in this article.

REFERENCES

[1] Çalık P, Takaç S, Çalık G, Özdamar TH. Serine alkaline protease overproduction capacity of *Bacillus licheniformis.* Enzyme Microb Tech 2000; 26: 45–60

[2] Massaiu I, Pasotti L, Sonnenschein N, Rama E, Cavaletti M, Magni P, Calvio C, Herrgård MJ. Integration of enzymatic data in *Bacillus subtilis* genome-scale metabolic model improves phenotype predictions and enables in silico design of poly-γ-glutamic acid production strains. *Microb Cell Fact* 2019;18:3

[3] Oh YK, Palsson BO, Park SM, Schilling CH, Mahadevan R. Genome-scale reconstruction of metabolic network in *Bacillus subtilis* based on high-throughput phenotyping and gene essentiality data. J Biol Chem 2007; 282: 28791-28799

[4] Wang H, Robinson JL, Kocabaş P, Gustafsson J, Anton M, Cholley PE, Huang S, Gobom J, Svensson T, Uhlen M et al. Genome-scale reconstruction of metabolic networks of model animals represents a platform for translational research. PNAS 2021; 118: 1-9

[5] Çalık P, Özdamar TH. Carbon sources affect metabolic capacities of *Bacillus* species for the production of industrial enzymes: theoretical analyses for serine and neutral proteases and α-amylase. Biochem Eng J 2001; 8: 61-81

[6] Çalık P, Özdamar TH. Bioreaction Network Flux Analysis For Industrial Microorganisms: A Review. Reviews in Chemical Engineering 2002; 18: 553-596

[7] Kunst F, Ogasawara N, Moszer I, Albertini AM, Alloni G, Azevedo V, Bertero MG, Bessieres P, Bolotin A, Borchert S et al. The complete genome sequence of the gram positive bacterium *Bacillus subtilis*. Nature 1997; 390: 249-256

[8] Barbe V, Cruveiller S, Kunst F, Lenoble P, Meurice G, Sekowska A, Vallenet D, Wang T, Moszer I, Medigue C et al. From a consortium sequence to a unified sequence: the *Bacillus subtilis* 168 reference genome a decade later. Microbiol 2009; 155: 1758-1775

[9] Belda E, Sekowska A, Le Fevre F, Morgat A, Mornico D, Ouzounis C, Vallenet D, Medigue C, Danchin A et al. An updated metabolic view of the *Bacillus subtilis* 168 genome. Microbiol 2013; 159: 757-770

[10] Borriss R, Danchin A, Harwood CR, Medigue C, Rocha EPC, Sekowska A, Vallenet D. *Bacillus subtilis*, the model Gram-positive bacterium: 20 years of annotation refinement. Microb Biotechnol 2018; 11: 3-17

[11] Geissler AS, Anthon C, Alkan F, González-Tortuero E, Poulsen LD, Kallehauge TB, Breüner A, Seemann SE, Vinther J, Gorodkin J. BSGatlas: a unified *Bacillus subtilis* genome and transcriptome annotation atlas with enhanced information access. Microb Genom 2021; 7:000524

[12] Kocabaş P, Çalık P, Çalık G, Özdamar TH. Analyses of extracellular protein production in *Bacillus subtilis*-I: Genome-scale metabolic model reconstruction based on updated gene-enzyme-reaction data. Biochemical Engineering Journal 2017; 127: 229-241

[13] Goelzer A, Brikci FB, Martin-Verstraete I, Noirot P, Bessières P, Aymerich S, Fromion V. Reconstruction and analysis of the genetic and metabolic regulatory networks of the central metabolism of *Bacillus subtilis*. BMC Syst Biol 2008; 2:20

[14] Henry CS, Zinner JF, Cohoon MP, Stevens RL. *i*Bsull03: A new genome-scale metabolic model of *Bacillus subtilis* based on SEED annotations. Genome Biol 2009; 10, R69

[15] Tanaka K, Henry CS, Zinner JF, Jolivet E, Cohoon MP, Xia F, Bidnenko V, Ehrlich SD, Stevens RL, Noirot P. Building the repertoire of dispensable chromosome regions in *Bacillus subtilis* entails major refinement of cognate large-scale metabolic model. Nucleic Acids Res 2013; 41: 687-699

[16] Hao T, Han B, Ma H, Fu J, Wang H, Wang Z, Tang B, Chen T, Zhao X. In silico metabolic

engineering of *Bacillus subtilis* for improved production of riboflavin Egl-237,(R,R)-2,3-butanediol and isobutanol. Mol Biosyst 2013; 9: 2034-2044

[17] Çalık P, Çalık G, Takaç S, Özdamar TH. Metabolic flux analysis for serinealkaline protease fermentation by *Bacillus licheniformis* in a defined medium: effects of oxygen transfer rate. Biotechnol Bioeng 1999; 64:151-167

[18] Heirendt L, Arreckx S, Pfau T, Mendoza SN, Richelle A, Heinken A, Haraldsdottir HS, Wachowiak J, Keating SM, Vlasov V et al. Creation and analysis of biochemical constraint-based models: the COBRA Toolbox v3.0. Nat Protoc 2019; 14: 639-702

[19] Sanchez BJ, Zhang C, Nilsson A, Lahtvee PJ, Kerkhoven EJ, Nielsen J. Improving the phenotype predictions of a yeast genome-scale metabolic model by incorporating enzymatic constriants. Mol Syst Biol 2017;13: 935

[20] Iacobazzi V, Infantino V. Citrate--New functions for an old metabolite. Biol Chem 2014; 395: 387-399

[21] Özdamar TH, Şentürk B, Yılmaz ÖD, Kocabaş P, Çalık G, Çalık P. Bioreaction network flux analysis for human protein producing *Bacillus subtilis* based on genome-scale model. Chemical Engineering Science 2010; 65: 574-580.